Electronic Supplementary Material (ESI) for Physical Chemistry Chemical Physics.

Supporting Information

Theoretical Insights into Effect of the Overpotentials on CO Electroreduction Mechanisms on Cu(111): Regulation and Application of Electrode Potentials from a CO Coverage-dependent Electrochemical Model

Lihui Ou[1*], Junxiang Chen[2]

1. Computational Details

1.1 Surface and Solvation Model

Considering the complexity of real CO_2 electroreduction systems, the aqueous-phase environment is included in the present study, in which 12 explicit H_2O molecules with two relaxed bilayer structures chosen to fill up the vacuum region were used to model the solvation effect in order to better simulate the interactions between solvent and adsorbates and decrease the size of the simulated systems as much as possible. In fact, the formation of an ordered H_2O bilayer structure in a hexagonal arrangement with 2/3 monolayer saturation coverage with respect to the surface normal had been demonstrated by X-ray absorption spectroscopy, thermal desorption spectroscopy, low-energy electron diffraction, X-ray photoelectron spectroscopy and scanning electron microscopy along with DFT calculations in previous experimental and theoretical studies on the meal surface.[1-3] Our present solvation model is on the basis of the previous studies on structure and orientation of H_2O. However, many different H_2O solvation structures may also exist, which all are approximate in energy.[4] Since all energies of interest in this study are energy differences, which are not sensitive to the accurate model of H_2O as long as the same model is consistently used and a reasonable model in a local minimum structure is choose when calculating the energy differences. Considering the coverage is 2/3 of H_2O monolayer, thus, a (3x3) Cu(111) slab model with nine metal atoms per layer and theoretical equilibrium lattice constant of 3.66 Å by using four metal layers was created.

*[1]*Hunan Province Cooperative Innovation Center for the Construction & Development of Dongting Lake Ecologic Economic Zone, College of Chemistry and Materials Engineering, Hunan University of Arts and Science, Changde, 415000, China. E-mail: oulihui666@126.com*

[2]*CAS Key Laboratory of Design and Assembly of Functional Nanostructures, Fujian Provincial Key Laboratory of Nanomaterials, Fujian Institute of Research on the Structure of Matter, Chinese Academy of Sciences, Fuzhou, 350002, China.*

2.2 Computational Parameters

Using the generalized gradient approximation of the Perdew–Burke–Ernzerhof exchange correlation functional, calculations were performed in the framework of DFT.[5] Ultrasoft pseudopotentials were employed to describe the nuclei and core electrons and the Kohn-Sam equations were self-consistently solved using a plane-wave basis set.[6] A kinetic energy cutoff of 30 Ry and a charge-density cutoff of 300 Ry were used to make the basis set finite. The Fermi surface has been treated by the smearing technique of Methfessel–Paxton with a smearing parameter of 0.02 Ry.[7] The PWSCF codes in Quantum ESPRESSO distribution were employed to perform all calculations.[8] Brillouin-zone integrations were implemented using a (3×3×1) uniformly shifted k-mesh for (3×3) supercell with the special-point technique, which was tested to converge to a subset of the relative energies reported herein. A vacuum layer of 16Å was placed above the top layer of slab, which is sufficiently large to ensure that the interactions are negligible between repeated slabs in a direct normal to the surface. The Cu atoms in the bottom two layers are fixed at the theoretical bulk positions, whereas the top two layers and all adsorbates including solvent are allowed to relax to minimize the total energy of the system. Structural optimization was performed until the Cartesian force components acting on each atom were brought below 10^{-3} Ry/Bohr and the total energy was converged to within 10^{-5} Ry. Using the climbing image nudged elastic band (CI-NEB) method, the saddle points and minimum energy paths (MEPs) were located.[9, 10] Zero point energy (ZPE) corrections were applied into the calculations of the activation and reaction energies from MEP analysis, in which density functional perturbation theory within the linear response was used to study the vibrational properties.[11] The ZPEs were calculated using the PHONONS code that contained in the Quantum ESPRESSO distribution.[8]

2. Conditions of Low Overpotentials

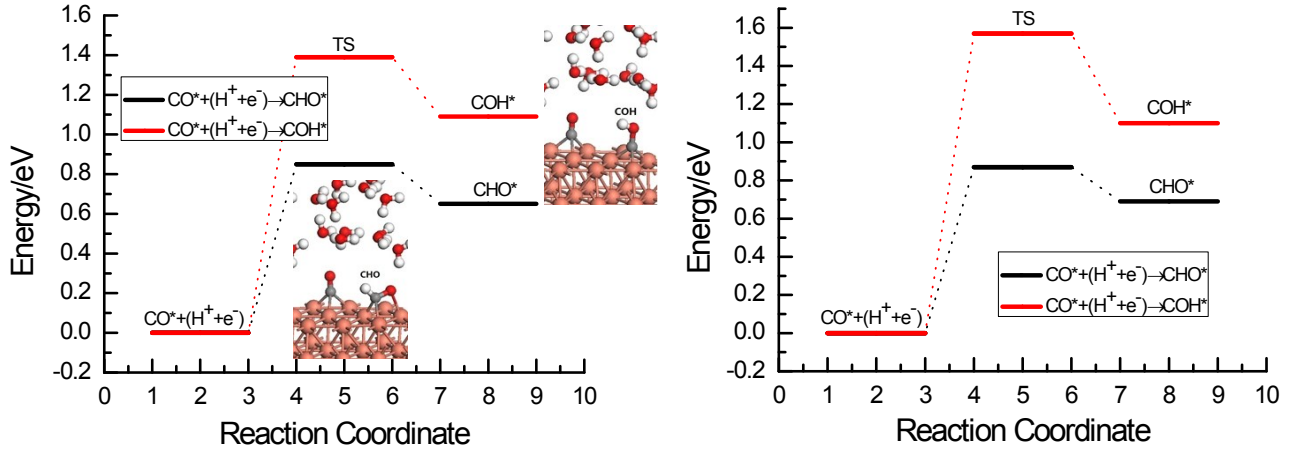

(a) (b)

Figure S1. The MEP analysis of CO electroreduction into CHO and COH intermediates on Cu(111) at the present simulated low overpotentials (an asterisk * indicates adsorption to the Cu surface): (a) 0.13 V; (b) 0.37 V.

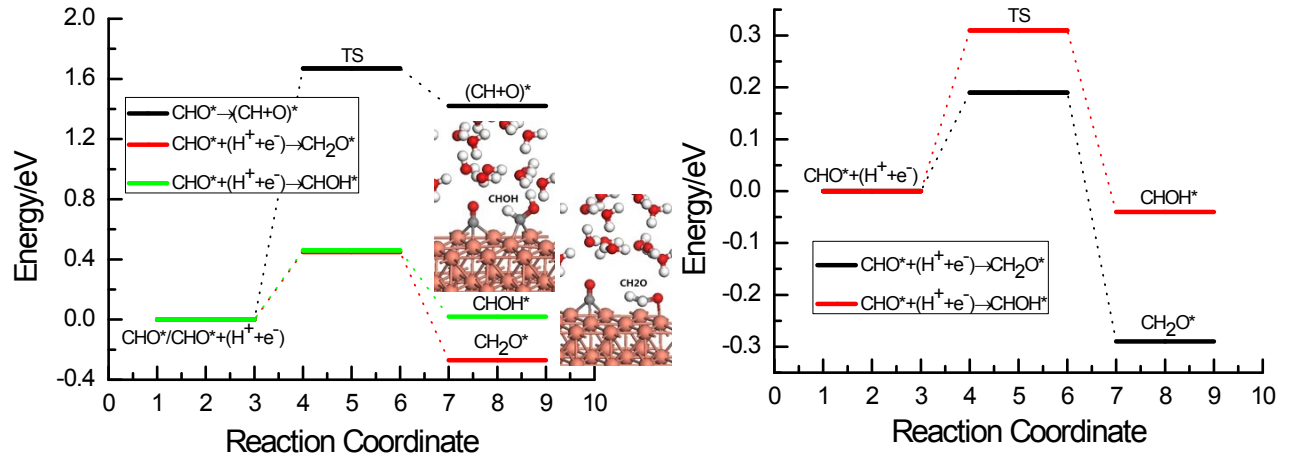

(a) (b)

Figure S2. The MEP analysis of CHO electroreduction into CH_2O and CHOH intermediates on Cu(111) at the present simulated low overpotentials: (a) 0.13 V; (b) 0.37 V.

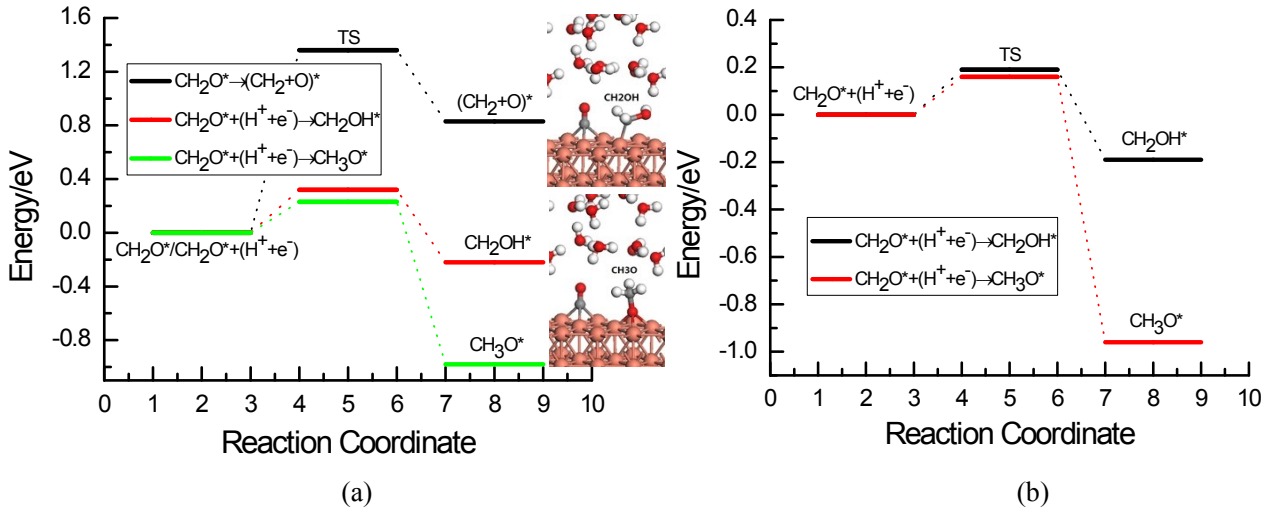

(a) (b)

Figure S3. The MEP analysis of CH_2O electroreduction into CH_2OH and CH_3O intermediates on Cu(111) at the present simulated low overpotentials: (a) 0.13 V; (b) 0.37 V.

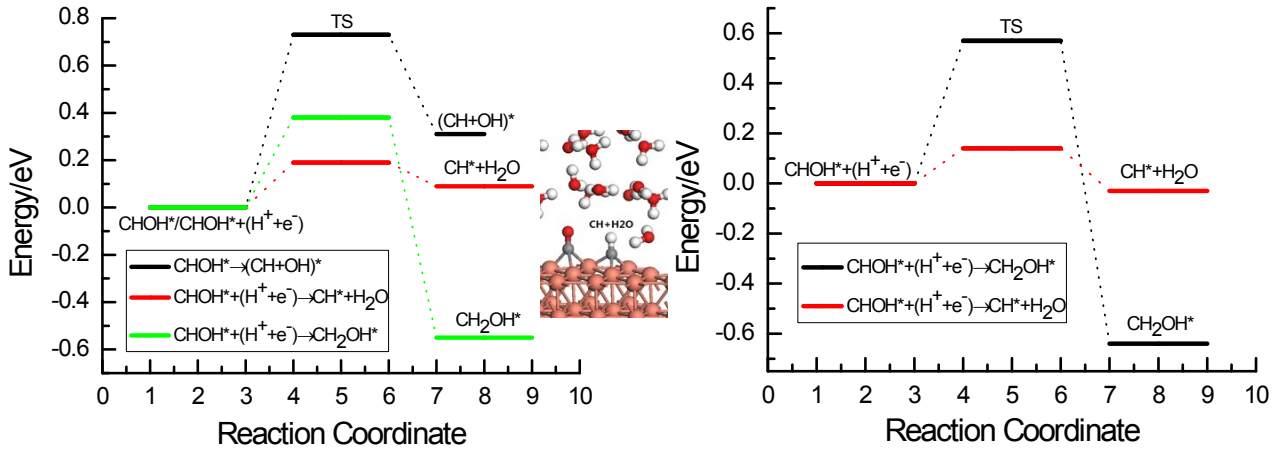

(a) (b)

Figure S4. The MEP analysis of CHOH electroreduction into CH_2OH and CH intermediates on Cu(111) at the present simulated low overpotentials: (a) 0.13 V; (b) 0.37 V.

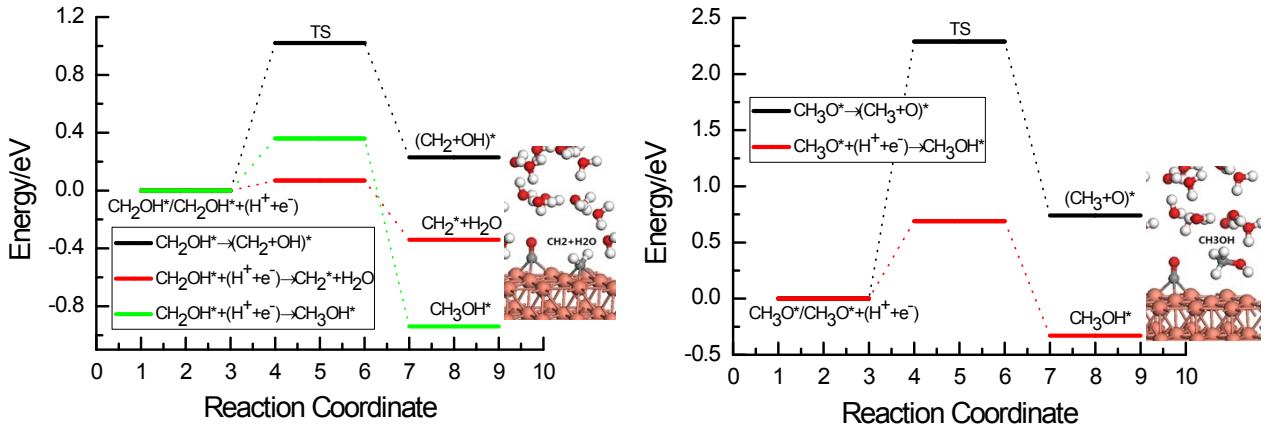

(a) (b)

Figure S5. The MEP analysis of (a) CH_2OH electroreduction into CH_2 intermediate and CH_3OH production and (b) CH_3O electroreduction into CH_3OH production on Cu(111) at the present simulated low overpotential of 0.13 V.

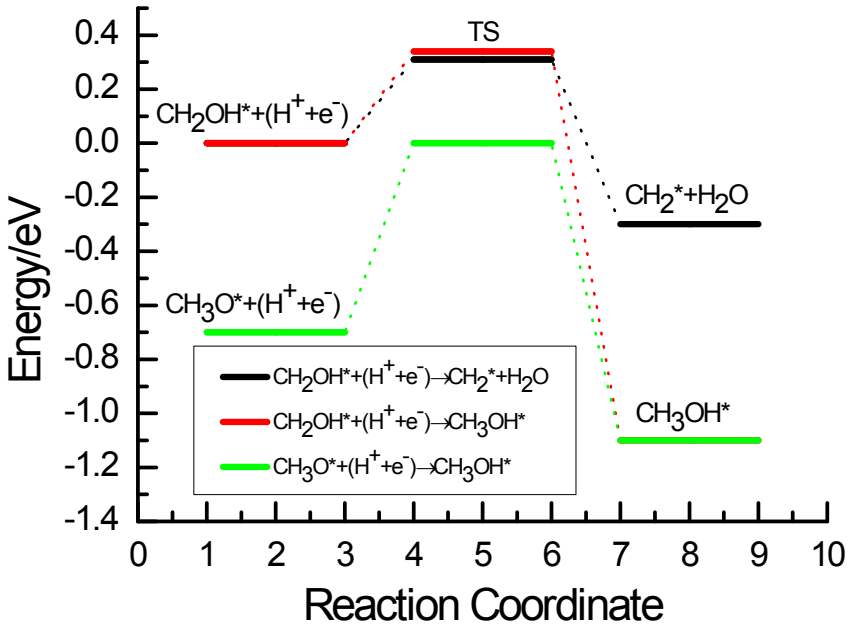

Figure S6. The MEP analysis of CH_2OH electroreduction into CH_2 intermediate and CH_3OH production and CH_3O electroreduction into CH_3OH production on Cu(111) at the present simulated low overpotential of 0.37 V.

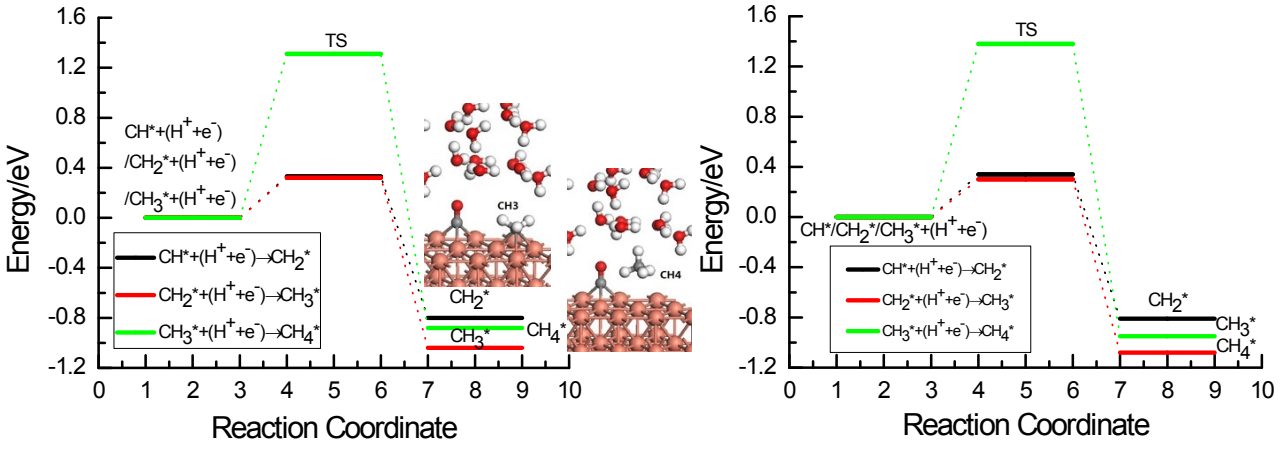

(a) (b)

Figure S7. The MEP analysis of CH electroreduction into CH_2, CH_2 electroreduction into CH_3 and CH_3 electroreduction into CH_4 on Cu(111) at the present simulated low overpotentials: (a) 0.13 V; (b) 0.37 V.

Table S1. Activation Barriers (ΔE_{act}, eV) and Reaction Free Energies (ΔG_{reac}, eV) for the Possible Elementary Reaction Steps for CO Electroreduction on Cu(111) in Aqueous Phase at the Low Overpotential of *ca*. 0.13 V

Reactions	ΔE_{act}, eV	ΔG_{reac}, eV[a]
$CO^* + (H^+ + e^-) \rightarrow CHO^*$	0.85	0.65
$CO^* + (H^+ + e^-) \rightarrow COH^*$	1.39	1.09
$CHO^* \rightarrow (CH + O)^*$	1.67	1.42
$CHO^* + (H^+ + e^-) \rightarrow CH_2O^*$	0.45	-0.27
$CHO^* + (H^+ + e^-) \rightarrow CHOH^*$	0.43	0.07
$CH_2O^* \rightarrow (CH_2 + O)^*$	1.36	0.83
$CH_2O^* + (H^+ + e^-) \rightarrow CH_2OH^*$	0.32	-0.22
$CH_2O^* + (H^+ + e^-) \rightarrow CH_3O^*$	0.23	-0.98
$CHOH^* \rightarrow (CH + OH)^*$	0.73	0.31
$CHOH^* + (H^+ + e^-) \rightarrow CH_2OH^*$	0.38	-0.55
$CHOH^* + (H^+ + e^-) \rightarrow CH^* + H_2O$	0.19	0.09
$CH_2OH^* \rightarrow (CH_2 + OH)^*$	1.02	0.23
$CH_2OH^* + (H^+ + e^-) \rightarrow CH_2^* + H_2O$	0.07	-0.34
$CH_2OH^* + (H^+ + e^-) \rightarrow CH_3OH^*$	0.36	-0.94
$CH_3O^* \rightarrow (CH_3 + O)^*$	2.29	0.74
$CH_3O^* + (H^+ + e^-) \rightarrow CH_3OH^*$	0.69	-0.33
$CH^* + (H^+ + e^-) \rightarrow CH_2^*$	0.33	-0.80
$CH_2^* + (H^+ + e^-) \rightarrow CH_3^*$	0.32	-1.04
$CH_3^* + (H^+ + e^-) \rightarrow CH_4^*$	1.31	-0.88

The asterisk (*) indicates that the species is adsorbed on Cu(111).

[a]In the calculations, the entropies obtained from the literature of Nørskov and coworkers are considered for gaseous molecules,[12, 13] whereas the entropies of the adsorbed species are ignored. The DFT calculated zero point energies (*ZPE*) for all species are included in the activation barrier and reaction free energy calculations.

Table S2. Activation Energies (ΔE_{act}, eV) and Reaction Free Energies (ΔG_{reac}, eV) for the Possible Elementary Reaction Steps for CO Electroreduction on Cu(111) in Aqueous Phase at the Low Overpotential of *ca*. 0.37 V

Reactions	ΔE_{act}, eV	ΔG_{reac}, eV
$CO^* + (H^+ + e^-) \rightarrow CHO^*$	0.87	0.69
$CO^* + (H^+ + e^-) \rightarrow COH^*$	1.57	1.10
$CHO^* + (H^+ + e^-) \rightarrow CH_2O^*$	0.19	-0.29
$CHO^* + (H^+ + e^-) \rightarrow CHOH^*$	0.31	-0.04
$CH_2O^* + (H^+ + e^-) \rightarrow CH_2OH^*$	0.19	-0.19
$CH_2O^* + (H^+ + e^-) \rightarrow CH_3O^*$	0.16	-0.96
$CHOH^* + (H^+ + e^-) \rightarrow CH_2OH^*$	0.57	-0.64
$CHOH^* + (H^+ + e^-) \rightarrow CH^* + H_2O$	0.14	-0.03
$CH_2OH^* + (H^+ + e^-) \rightarrow CH_2^* + H_2O$	0.31	-0.30
$CH_2OH^* + (H^+ + e^-) \rightarrow CH_3OH^*$	0.34	-0.98
$CH_3O^* + (H^+ + e^-) \rightarrow CH_3OH^*$	0.70	-0.40
$CH^* + (H^+ + e^-) \rightarrow CH_2^*$	0.34	-0.81
$CH_2^* + (H^+ + e^-) \rightarrow CH_3^*$	0.30	-1.08
$CH_3^* + (H^+ + e^-) \rightarrow CH_4^*$	1.38	-0.95

3. Conditions of High Overpotentials

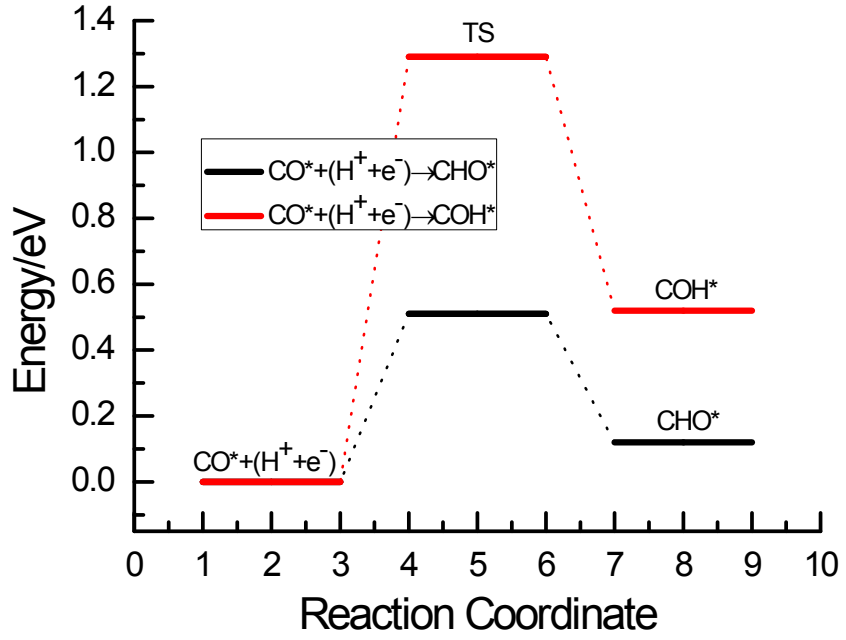

Figure S8. The MEP analysis of CO electroreduction into CHO and COH intermediates on Cu(111) at the present simulated high overpotentials of *ca*. 0.80 V (an asterisk * indicates adsorption to the Cu surface).

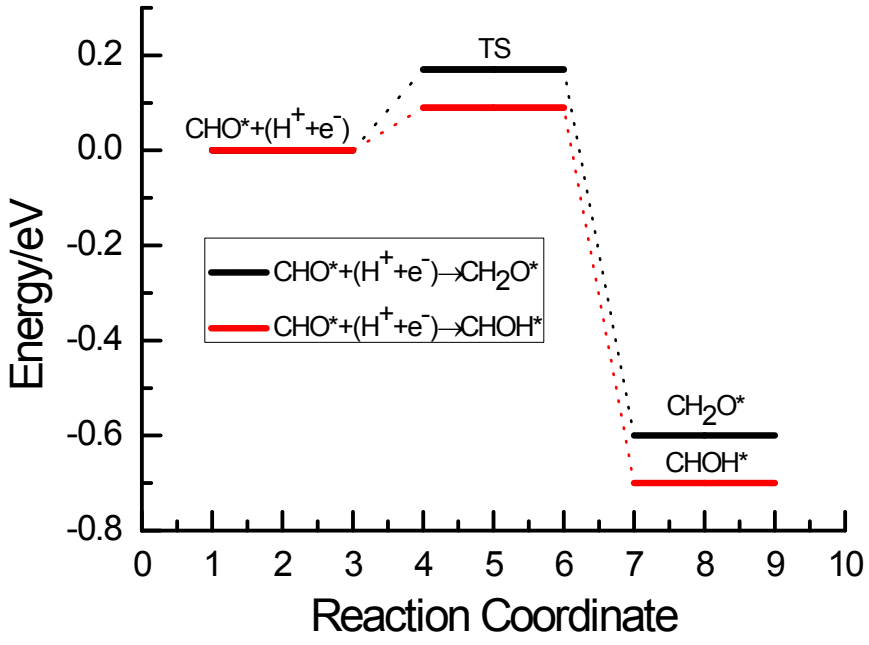

Figure S9. The MEP analysis of CHO electroreduction into CH_2O and CHOH intermediates on Cu(111) at the present simulated high overpotentials of *ca*. 0.80 V.

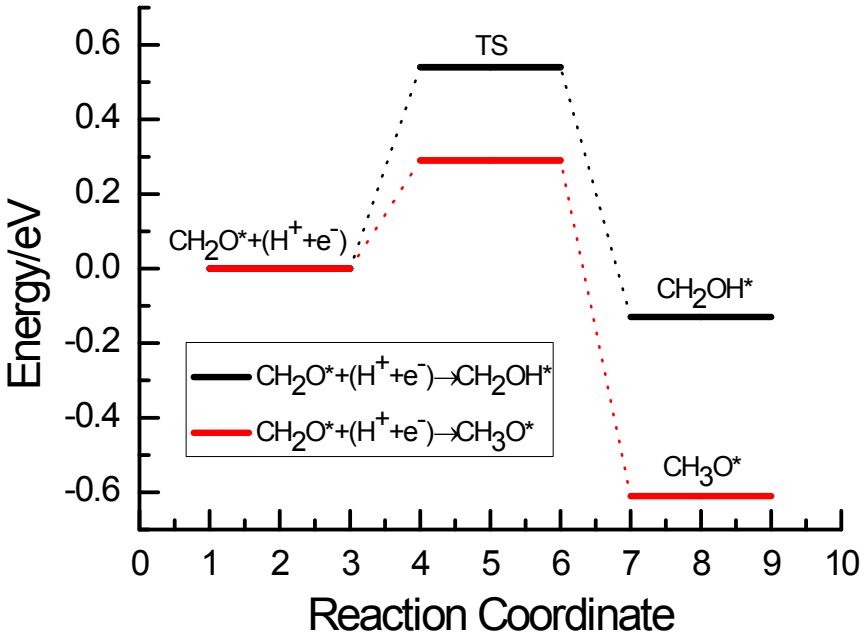

Figure S10. The MEP analysis of CH_2O electroreduction into CH_2OH and CH_3O intermediates on Cu(111) at the present simulated high overpotentials of *ca*. 0.80 V.

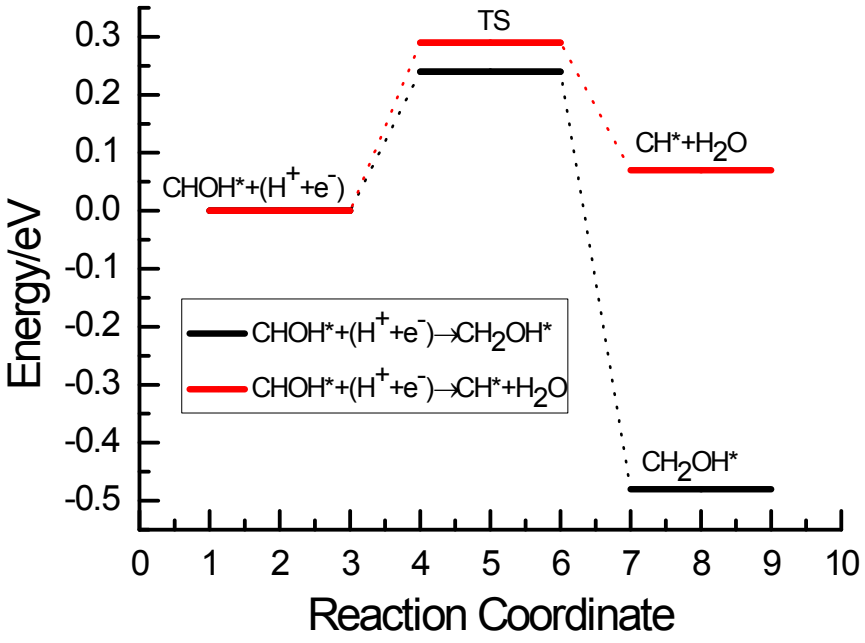

Figure S11. The MEP analysis of CHOH electroreduction into CH_2OH and CH intermediates on Cu(111) at the present simulated high overpotentials of *ca*. 0.80 V.

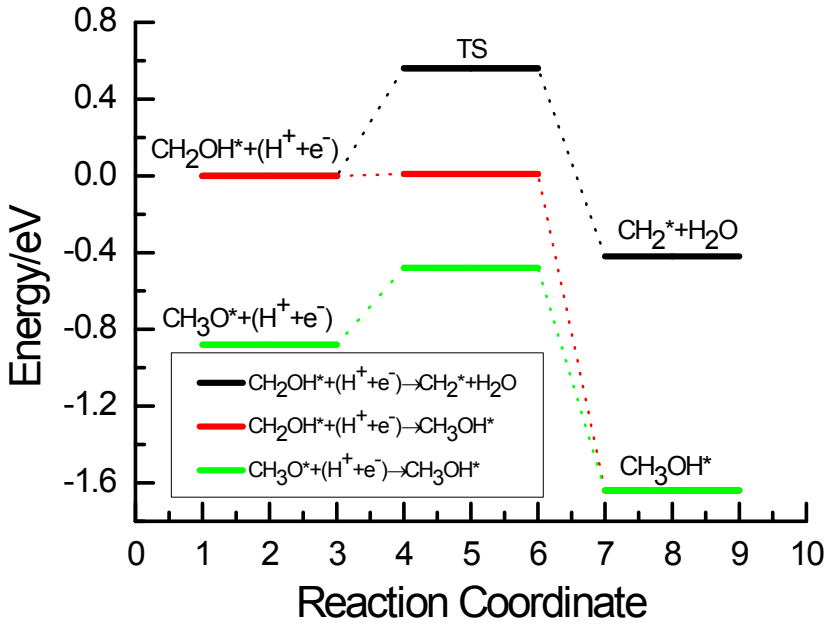

Figure S12. The MEP analysis of CH_2OH electroreduction into CH_2 intermediate and CH_3OH production and CH_3O electroreduction into CH_3OH production on Cu(111) at the present simulated high overpotential of *ca*. 0.80 V.

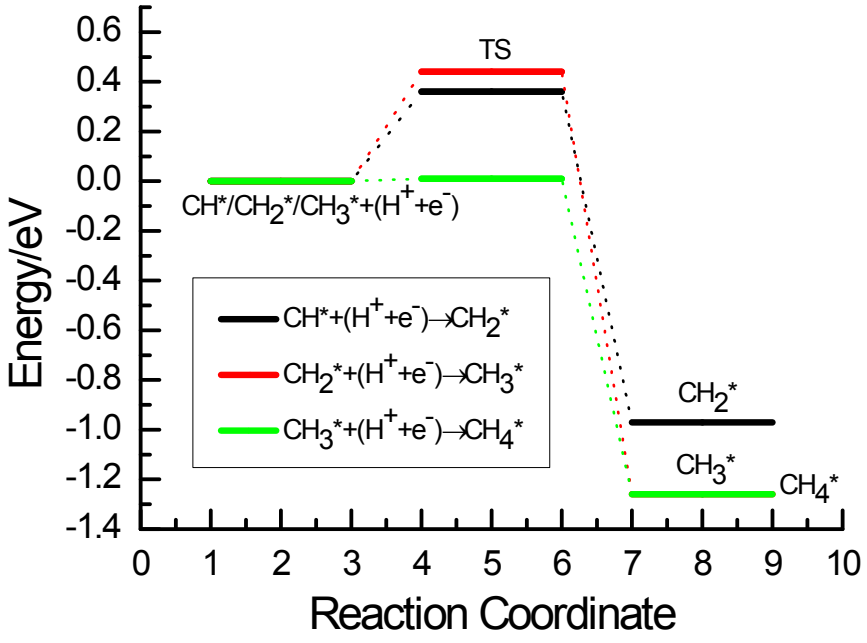

Figure S13. The MEP analysis of CH electroreduction into CH_2, CH_2 electroreduction into CH_3 and CH_3 electroreduction into CH_4 on Cu(111) at the present simulated high overpotential of *ca*. 0.80 V.

Table S3. Activation Energies (ΔE_{act}, eV) and Reaction Free Energies (ΔG_{reac}, eV) for the Possible Elementary Reaction Steps for CO Electroreduction on Cu(111) in Aqueous Phase at the High Overpotential of *ca*. 0.80 V

Reactions	ΔE_{act}, eV	ΔG_{reac}, eV
$CO^* + (H^+ + e^-) \rightarrow CHO^*$	0.51	0.12
$CO^* + (H^+ + e^-) \rightarrow COH^*$	1.29	0.52
$CHO^* + (H^+ + e^-) \rightarrow CH_2O^*$	0.17	-0.60
$CHO^* + (H^+ + e^-) \rightarrow CHOH^*$	0.09	-0.70
$CH_2O^* + (H^+ + e^-) \rightarrow CH_2OH^*$	0.54	-0.13
$CH_2O^* + (H^+ + e^-) \rightarrow CH_3O^*$	0.29	-0.61
$CHOH^* + (H^+ + e^-) \rightarrow CH_2OH^*$	0.24	-0.48
$CHOH^* + (H^+ + e^-) \rightarrow CH^* + H_2O$	0.29	0.07
$CH_2OH^* + (H^+ + e^-) \rightarrow CH_2^* + H_2O$	0.56	-0.42
$CH_2OH^* + (H^+ + e^-) \rightarrow CH_3OH^*$	0.01	-1.64
$CH_3O^* + (H^+ + e^-) \rightarrow CH_3OH^*$	0.40	-0.76
$CH^* + (H^+ + e^-) \rightarrow CH_2^*$	0.36	-0.97
$CH_2^* + (H^+ + e^-) \rightarrow CH_3^*$	0.44	-1.26
$CH_3^* + (H^+ + e^-) \rightarrow CH_4^*$	0.01	-1.26

References

(1) E. Skúlason, V. Tripković, M. E. Björketun, S. Gudmundsdóttir, G. Karlberg, J. Rossmeisl, T. Bligaard, H. Jónsson and J. K. Nørskov, Modeling the Electrochemical Hydrogen Oxidation and Evolution Reactions on the basis of Density Functional Theory Calculations, *J. Phys. Chem. C*, 2010, **114**, 18182-18197.

(2) M. A. Henderson, Interaction of Water with Solid surfaces: Fundamental Aspects Revisited, *Surf. Sci. Rep*., 2002, **46**, 1-308.

(3) H. Ogasawara, B. Brena, D. Nordlund, M. Nyberg, A. Pelmenschikov, L. G. M. Pettersson and A. Nilsson, Structure and Bonding of Water on Pt(111), *Phys. Rev. Lett*., 2002, **89**, 276102.

(4) S. Haq, C. Clay, G. R. Darling, G. Zimbitas and A. Hodgson, Growth of Intact Water Ice on Ru(0001) between 140 and 160 K: Experiment and Density-Functional Theory Calculations, *Phys. Rev. B*, 2006, **73**, 115414.

(5) J. P. Perdew, K. Burke and M. Ernzerhof, Generalized Gradient Approximation Made Simple, *Phys. Rev. Lett*., 1996, **77**, 3865-3868.

(6) D. Vanderbilt, Soft Self-Consistent Pseudopotentials in a Generalized Eigenvalue Formalism, *Phys. Rev. B*, 1990, **41**, 7892-7895.

(7) M. Methfessel and A. T. Paxton, High-Precision Sampling for Brillouin-Zone Integration in Metals. *Phys. Rev. B*, 1989, **40**, 3616-3621.

(8) S. Baroni, A. Dal Corso, S. de Gironcoli and P. Giannozzi, PWSCF and PHONON: Plane-Wave Pseudo-Potential Codes, http://www.quantum-espresso.org/, **2001**.

(9) G. Henkelman and H. Jonsson, Improved Tangent Estimate in the Nudged Elastic Band Method for Finding Minimum Energy Paths and Saddle Points, *J. Chem. Phys*., 2000, **113**, 9978-9985.

(10) G. Henkelman, B. P. Uberuaga and H. Jonsson, A Climbing Image Nudged Elastic Band Method for Finding Saddle Points and Minimum Energy Paths, *J. Chem. Phys*., 2000, **113**, 9901-9904.

(11) S. Baroni, S. Gironcolli, A. Corso and P. Giannozzi, Phonons and Related Properties of Extended Systems from Density Functional Perturbation Theory, *Rev. Mod. Phys*., 2001, **73**, 515-562.

(12) A. A. Peterson, F. Abild-Pederson, F. Studt, J. Rossmeisl and J. K. Nørskov, How Copper Catalyzes the Electroduction of Carbon Dioxide into Hydrocarbon Fuels, *Energy Environ. Sci*., 2010, **3**, 1311-1315.

(13) W. J. Durand, A. A. Peterson, F. Studt, F. Abild-Pederson and J. K. Nørskov, Structure Effects on the Energetics of the Electrochemical Reduction of CO_2 by Copper Surfaces, *Surf. Sci*., 2011, **605**, 1354-1359.